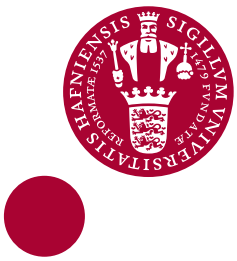

Induced Mesocrystal-Formation, Hydrothermal Growth and Magnetic Properties of alpha-Fe2O3 Nanoparticles in Salt-Rich Aqueous Solutions

Brok, Erik; Larsen, Jacob; Varón, Miriam; Hansen, Thomas W.; Frandsen, Cathrine

Published in:
Crystals

DOI:
10.3390/cryst7080248

Publication date:
2017

Document version
Publisher's PDF, also known as Version of record

crystals

MDPI

Article

Induced Mesocrystal-Formation, Hydrothermal Growth and Magnetic Properties of α-Fe_2O_3 Nanoparticles in Salt-Rich Aqueous Solutions

Erik Brok [1,2,3,4,5], Jacob Larsen [1], Miriam Varón [1], Thomas W. Hansen [2] and Cathrine Frandsen [1,*]

1 Department of Physics, Technical University of Denmark, DK-2800 Kgs. Lyngby, Denmark; e.brok@nbi.ku.dk (E.B.); jacb@fysik.dtu.dk (J.L.); mirva@fysik.dtu.dk (M.V.)
2 Center for Electron Nanoscopy, Technical University of Denmark, DK-2800 Kgs. Lyngby, Denmark; thomas.w.hansen@cen.dtu.dk
3 NIST Center for Neutron Research, National Institute of Science and Technology, Gaithersburg, MD 20899, USA
4 Department of Materials Science and Engineering, University of Maryland, College Park, MD 20742, USA
5 Nano-Science Center, Niels Bohr Institute, University of Copenhagen, Universitetsparken 5, DK-2100 Copenhagen, Denmark
* Correspondence: fraca@fysik.dtu.dk; Tel.: +45-45253167

Academic Editor: Monica Distaso
Received: 15 June 2017; Accepted: 21 July 2017; Published: 8 August 2017

Abstract: Iron oxide nanoparticles are widely prevalent in our aqueous environment (e.g., streams, seawater, hydrothermal vents). Their aggregation and crystal growth depend on their chemical surroundings, for instance just a change in pH or salt concentration can greatly affect this. In turn this influences their properties, mobility, fate, and environmental impact. We studied the growth of α-Fe_2O_3 (hematite), starting from 8 nm hematite particles in weakly acidic (HNO_3) aqueous suspension with different states of particle aggregation, using salt (NaCl and NaH_2PO_4) to control their initial aggregation state. The samples were then subject to hydrothermal treatment at 100–140 °C. We followed the development in aggregation state and particle size by dynamic light scattering, X-ray diffraction, small angle neutron scattering and transmission electron microscopy, and the magnetic properties by Mössbauer spectroscopy. The addition of NaCl and NaH_2PO_4 both led to aggregation, but NaCl led to linear chains of hematite nanoparticles (oriented parallel to their hexagonal c-axis), such that the crystalline lattice planes of neighboring hematite particles were aligned. However, despite this oriented alignment, the particles did not merge and coalesce. Rather they remained stable as mesocrystals until heat-treated. In turn, the addition of NaCl significantly increases the rate of growth during hydrothermal treatment, probably because the nanoparticles, due to the chain formation, are already aligned and in close proximity. With hydrothermal treatment, the magnetic properties of the particles transform from those characteristic of small (aggregated) hematite nanoparticles to those of particles with more bulk-like properties such as Morin transition and suppression of superparamagnetic relaxation, in correspondence with the growth of particle size.

Keywords: mesocrystals; aggregation; hydrothermal crystal growth; α-Fe_2O_3; hematite; magnetic nanoparticles; Morin transition; magnetic relaxation

1. Introduction

Within the last decades, it has become clear that aggregation-based crystal growth is an important growth mechanism for nanoparticles in solutions [1–3]. Moreover, it is also clear that this growth mechanism often leads to meta-stable anisotropic particle structures such as chains or hierarchical

structures of attached particles [1,4,5]. These structures (e.g., particle chains) are often taken as strong evidence that crystal growth is governed by aggregation [1,2].

The driving mechanism, which can lead to oriented crystalline attachment between particles, can be Coulombic interactions between surface atoms of nanoparticles [3,6], while electrostatic repulsion between particles, e.g., tuned by pH (low or high), can be used to maintain a stable particle suspension. By adding ligands and passivating agents, or otherwise changing the particle surface, one can control the growth [5]. There are several studies about colloidal nanoparticles and their local environment, which show effects of addition of ions in the synthesis and the changed stability of otherwise ligand-free nanoparticles. For instance salt in solution screens the charge on the nanoparticle surface, and thus typically leads to colloidal instability followed by aggregation [7,8]. It is however not so well understood at the nanoscale how addition of salt may specifically affect the attachment and crystal growth process. Changing the ionic strength by addition of salts may change not only the isotropic repulsive potential between the nanoparticles, but also result in anisotropic changes due to preferential adsorption of ions on specific surfaces. By this mechanism, preferred absorption could be used to induce oriented attachment of nanoparticles.

In studies of crystal growth, governed by addition of ions, rather than by particle aggregation, it has been found that growth can be retarded or preferred in certain directions due to addition of specific ions. In case of hematite (α-Fe_2O_3), it has been shown that anions such as Cl^-, OH^-, $SO_4{}^{2-}$, and $PO_4{}^{3-}$ have remarkably different effects on the morphology of hematite particles grown by forced hydrolysis, due to preferred adsorption of anions [9–11]. Also, Livage et al. and Reeves et al. have demonstrated the influence of inorganic ions such as Cl^-, $NO_3{}^-$ and $ClO_4{}^-$ on the shape and size of hematite and other transition metal oxides [12,13].

Here we study, at the nanoscale, the aggregation of 8 nm hematite (α-Fe_2O_3) particles in acidic aqueous suspensions, with different concentrations of NaCl and NaH_2PO_4. Subsequently, the samples were exposed to hydrothermal treatment such that the effect on growth due to aggregation prior to hydrothermal treatment could be investigated.

The use of NaCl was inspired by studies of He et al. [14] who showed aggregation of hematite nanoparticles after NaCl addition, but no nanoscopic details of the particle arrangement. Sugimoto et al. [9] and others used NaH_2PO_4 to control particle morphology during growth of hematite, and animated by this we chose NaH_2PO_4 as a complementary salt to affect aggregation.

Hematite is a common, naturally occurring mineral and the most stable of the iron oxides (often seen in red soils). It crystallizes in the corundum structure (space group $R\bar{3}c$). The magnetic structure of hematite is antiferromagnetic below its Néel temperature of T_N = 955 K [15]. At a temperature $T_M \approx 264$ K [16,17], known as the Morin temperature, hematite undergoes a spin-flop transition in which the spin orientation changes from close to the basal (001) plane to along the hexagonal c-axis. Between T_N and T_M, hematite is a canted antiferromagnet with a small magnetization (0.4 Am^2/kg).

Magnetic interactions between particles may play a role in driving oriented attachment. Obviously magnetic dipole interactions can be important for ferro- or ferrimagnetic particles and can lead to chain structures and even two- and three dimensional structures [18]. As antiferromagnetic materials do not possess a net magnetization they are not expected to have any magnetic dipole moment, although, because of a significant fraction of uncompensated spins, this is not strictly true for nanoparticles of antiferromagnetic materials. However, for 8 and 20 nm hematite particles, magnetic dipolar interactions are found to be negligible [19–21].

Despite its short range, exchange interactions can conceivably play a role in the attachment process. Frandsen et al. [21] estimate the exchange interaction between surfaces of hematite particles in some cases to be comparable to the chemical surface energy and hence it is possible that the exchange interaction can be partly responsible for the observed tendency for hematite particles to attach preferentially on certain faces.

In this study of 8 nm hematite particles, we do not anticipate magnetism to be a driving force for the aggregation-based crystal growth, but we follow the development in magnetic properties during

different aggregation states and particle growth, as magnetic changes are indicative of the aggregation and growth. For instance, hematite particles smaller than 20 nm typically show superparamagnetic behavior (fast magnetic relaxation), but this tends to be suppressed by inter-particle exchange interactions [19–21]. Moreover, the Morin temperature is known to be significantly lowered for particles smaller than 1 μm and the Morin transition is absent at temperatures down to 4.2 K in particles smaller than 20 nm [15].

2. Materials and Methods

The as-prepared sample of monodisperse hematite particles in aqueous suspension was produced by a sol-gel method similar to that described by Sugimoto et al. [9], Frandsen et al. [21] and Gilbert et al. [22]. The particles were suspended in dilute HNO_3 (pH ≈ 3.9) which provides an electrostatic charging of the particles such that the suspension is very stable with a zeta-potential $\zeta > 50$ mV. Sample concentration of the as-prepared sample is ~2 mg Fe/mL.

Small volumes (2 mL) of as-prepared sample were mixed 1:1 with solutions of 0 to 5.0 mM NaCl in H_2O or 0.0013 mM to 2.5 mM NaH_2PO_4 in H_2O, yielding samples with NaCl concentrations of 0–2.5 mM and samples with NaH_2PO_4 concentrations of 0.0007–1.25 mM. Here, the unit M is mole per liter (mole/L). NaCl dissolves as Na^+ and Cl^-. NaH_2PO_4 dissolved in water is weakly acidic (mainly due to dihydrogen-phosphate, $H_2PO_4^-$); when mixed with the nanoparticle suspension (pH ~3.9), we expect $H_2PO_4^-$ to remain as the predominant phosphate ion. The as-prepared sample, with and without added salts, was heated in PTFE lined autoclaves for 10 days at 100 °C, 120 °C, or 140 °C.

Transmission electron microscopy (TEM) images of the samples, drop-casted and dried on lacey carbon copper grids coated with ultrathin amorphous carbon, were obtained by an FEI Tecnai microscope. High-resolution TEM micrographs were obtained by an FEI Titan E Cell 80 300ST microscope.

X-ray diffraction (XRD) patterns were collected on a PanAnalytical diffractometer with a Cu-K_α source. The XRD samples were prepared by drying the suspension onto a Si sample holder.

Dynamic light scattering (DLS) measurements on sample suspensions were carried out by use of a Malvern ZetasizerNano.

Small angle neutron scattering (SANS) experiments were performed on the as-prepared sample and a sample with 2.5 mM NaCl which had not been autoclaved, on the NG7SANS instrument at the NIST Center for Neutron Research. Three detector configurations (1 m, 4 m and 13 m) were used with neutrons of wavelength $\lambda = 6.0$ Å, spanning a q-range from approximately 0.004 $Å^{-1}$ to 0.4 $Å^{-1}$. Data reduction (background subtraction, scaling, and circular averaging) were performed using the NCNR Igor programs [23] and data analysis was performed using the SasView software [24]. Approximately 0.6 mL of sample was loaded in standard 1 mm path length titanium cells with quartz windows and placed in the sample chamber. A magnet used in a previous experiment produced a magnetic field of 110 mT at the sample position, which should have no appreciable influence on the suspensions of hematite particles.

Mössbauer spectra were measured on sample suspensions flash frozen in liquid N_2. The spectra were obtained using a constant-acceleration spectrometer, cryogen-free cooling down to 18 K, and a source of ^{57}Co in Rh. The spectra were calibrated using α-Fe foil. Because of the relatively low concentration of particles in the suspension the Mössbauer absorption was quite low (1–3%) and to obtain significant statistics the samples were typically measured for 48–72 hours. The spectral components were fitted with Lorentzian lines; the magnetically split parts with sextets with line area ratio 3:2:1:1:2:3, the superparamagnetic relaxed parts with unconstrained single Lorentzian lines.

3. Results

3.1. The As-Prepared Sample

Figure 1 shows a representative TEM image of the as-prepared sample of hematite nanoparticles. Generally, the images show rather well dispersed particles but also some aggregates of particles that may be an effect of the drying process. The particle edges are soft and irregularly shaped, without pronounced crystal facets. The dispersed particles often appear elongated in shape and often with morphology as if they were small chains of ~2–4 coalesced subparticles. The particle size in the longest direction and in the direction perpendicular to the longest direction were measured for 45 particles giving an average particle length of 14 ± 2 nm and a particle width of 8 ± 2 nm, where ±2 denotes the standard deviation of the average (all given uncertainties are the estimated standard deviations).

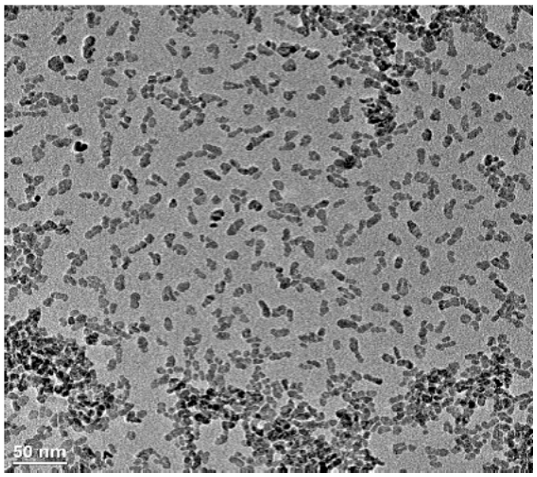

Figure 1. TEM image of the as-prepared α-Fe_2O_3 nanoparticle sample.

Figure 2 shows XRD measurements of the as-prepared sample. The diffraction pattern shows the expected peaks of the hematite structure and no detectable peaks from other structures. Rietveld refinement of the $R\bar{3}c$ structure of hematite was performed in WINPOW, a modified version of the LHMP1 program [25]. Voigtian line shapes were used, assuming a Lorentzian broadening from the sample and a Gaussian instrumental broadening. The disagreements between the calculated and observed diffraction patterns are primarily due to misfits of the peak shape due to this assumption. The refinement results in unit cell parameters of a = 5.0417 ± 0.00004 Å and c = 13.7900 ± 0.0007 Å and a mean particle size of 9.5 ± 0.3 nm. A refinement of a model with two particle size parameters was performed to obtain information about the particle size in the [001] direction and perpendicular to [001], resulting in particle sizes of about 10.2 nm in the [001] direction and 8.2 nm perpendicular to [001]. However, these refined particle sizes depend delicately on details in the refined model (e.g., changing the number of background parameters) and their values should not be taken as accurate, but the size in the [001] direction is consistently refined as larger than in the perpendicular direction.

Our TEM and XRD results on the size and morphology of the as-prepared sample are in agreement with previous studies of hematite nanoparticles prepared by a similar method [21,22]; in these studies, it was found by high resolution TEM and X-ray investigations that the particles on average are elongated about 40% in the hexagonal [001] direction.

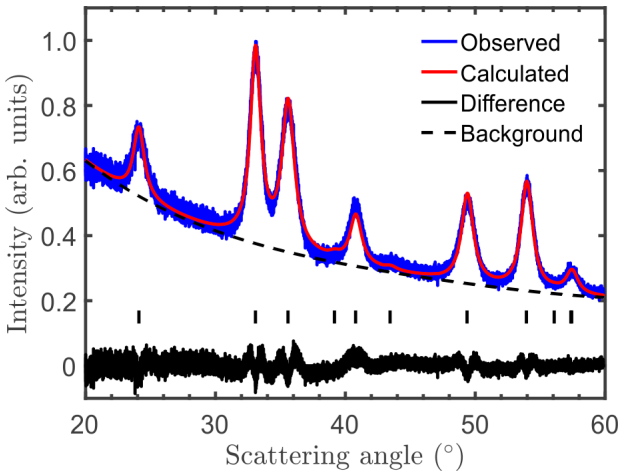

Figure 2. XRD pattern of the as-prepared sample. The tick marks correspond to the $R\bar{3}c$ structure of hematite.

3.2. *Effect of Salt Concentration: Aggregation*

Figure 3 shows TEM images of the sample of hematite nanoparticles with 2.5 mM NaCl. The chains consist of particles similar to those observed in the as-prepared sample (Figure 1), but the images suggest that the particles, when in the NaCl rich environment, form a network of long, rather straight, chains. Some chains are several hundred nanometers long consisting of dozens of particles. The particles in the chains are not fused together and there may be solvent molecules between the particles. The as-prepared particles (Figure 1), or those with lower concentrations than 2.5 mM NaCl (not shown), show no such aggregation effect at the time-scale studied.

The aggregation in the sample with 2.5 mM NaCl tends to be preferentially with the long [001] axes of the particles aligned, tentatively indicating that the attachment is often crystallographically oriented. This has been confirmed by high-resolution TEM images. One representative example is shown in Figure 4a. In the presented image, the most prominent lattice fringes are the ones parallel to the length of the elongated particle in the upper left corner, which is also shown in the enlarged image (Figure 4b). The periodicity of the fringes is 2.5 Å corresponding to the d-spacing of the hematite (110) planes. Since the (110) planes are perpendicular to [001] this confirms that the particles are elongated in the [001] direction. Furthermore, high-resolution TEM shows that the alignment of the lattice planes continues from one particle to the next even though there appears to be a gap between the particles (Figure 4b). This particle configuration remains very stable over time (months).

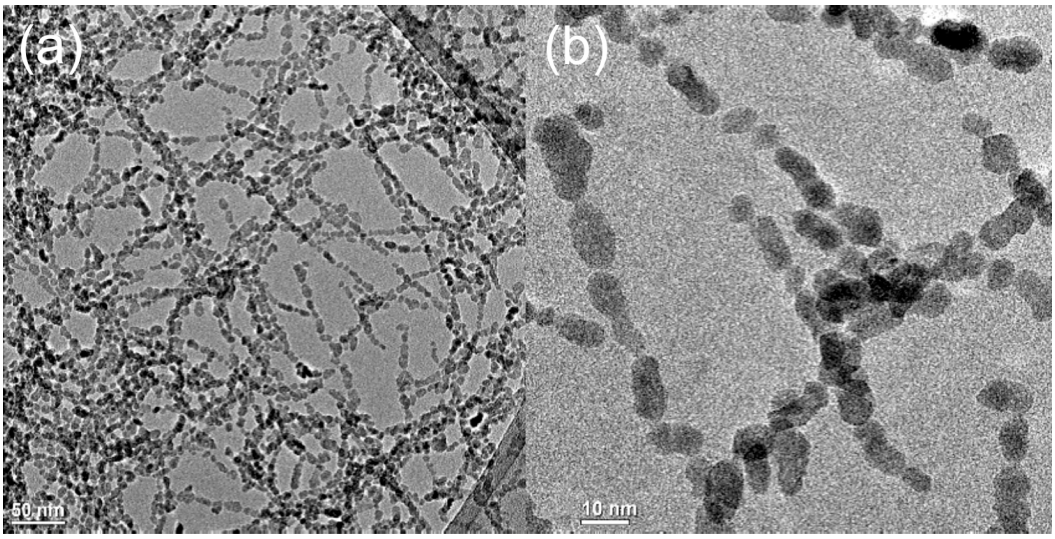

Figure 3. TEM images of the α-Fe_2O_3 nanoparticle sample with 2.5 mM NaCl; (**b**) is enlarged view of part of (**a**).

Potentially, one could speculate that the chains might not be present in the aqueous suspension but be an effect of drying e.g., of NaCl crystallisation during drying. However, as outlined below, data from DLS (Figure 5) and SANS (Figure 6) obtained on the 2.5 mM NaCl liquid sample show that the hematite chains are present in the suspensions.

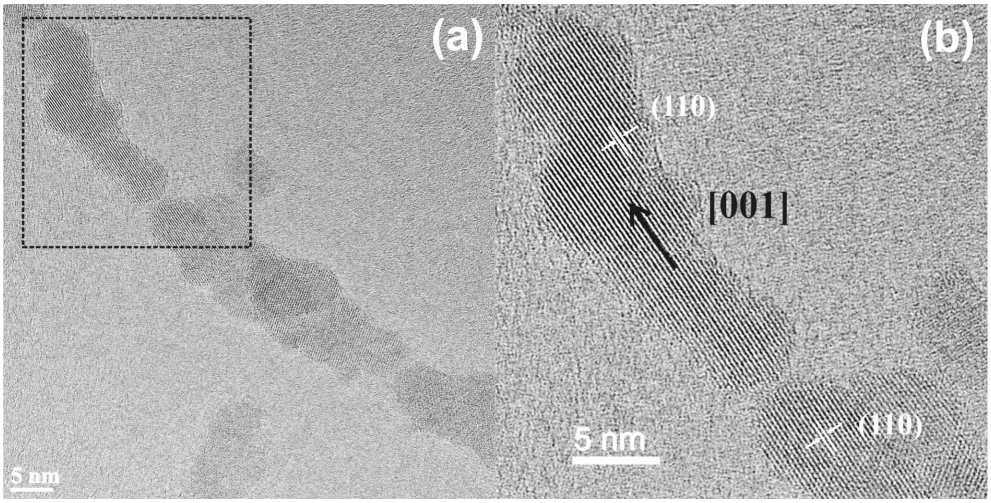

Figure 4. High-resolution TEM images of the hematite nanoparticle sample with 2.5 mM NaCl. (**a**) Image of a chain of hematite particles with lattice planes of neighboring particles aligned; (**b**) Enlarged view of the selected area in (a). The spacing between the lattice fringes corresponds to the (110) d-spacing.

Figure 5 shows the particle size distributions (PSDs) measured by DLS for the as-prepared sample and three different concentrations of NaCl. Intensity, volume and number distributions of the particle size (hydrodynamic diameter d_H) are shown. The intensity PSD (Figure 5a) shows one well-defined peak centered at d_H = 22 $\pm$ 12 nm (here $\pm$ denotes the width of the distribution) for the as-prepared sample. The volume and number distribution (Figure 5b,c) gives hydrodynamic diameters of d_H = 11.8 $\pm$ 5.2 nm and d_H = 8.8 $\pm$ 2.6 for the as-prepared sample. The PSDs for the samples with NaCl concentrations up to 0.5 mM are essentially identical to that of the as-prepared

sample, showing that addition of NaCl at these concentrations does not lead to aggregation during the time scales studied (6 months), confirming the findings with TEM. However, in the sample with a 2.5 mM NaCl concentration the DLS data looks very different. The intensity PSD of this sample spans more than an order of magnitude and produces a hydrodynamic diameter of d_H = 352 ± 338 nm. The very high polydispersity means that the sample is not ideally suited for DLS measurements and the determined PSD is not necessarily accurate and it makes no sense to convert the intensity PSD to volume or number distributions. From this it is clear that aggregation takes place in solution following addition of NaCl at a 2.5 mM concentration.

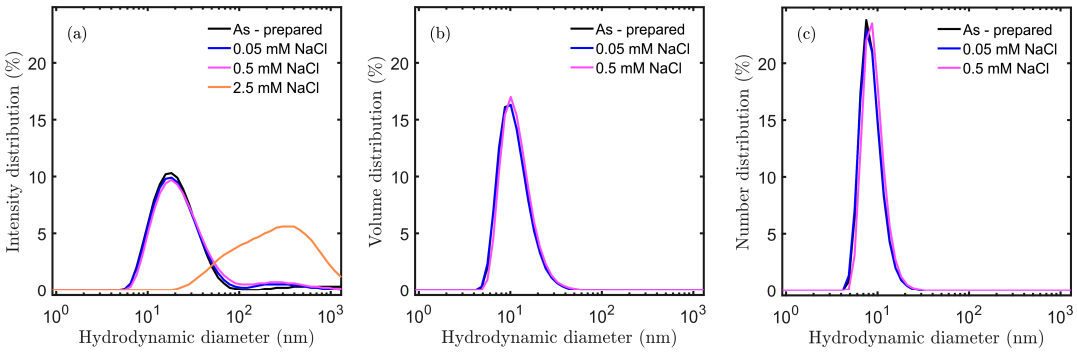

Figure 5. Particle size distributions (PSDs) measured with dynamic light scattering (DLS) before hydrothermal treatment. (**a**) Size distribution by intensity; (**b**) Size distribution by volume; (**c**) Size distribution by numbers.

SANS data obtained on the as-prepared sample and the sample with 2.5 mM NaCl are shown in Figure 6. The two SANS curves are distinctly different.

The SANS data from the as-prepared sample (Figure 6a) could be modelled relatively well with asymmetric geometric shapes such as cylinders or ellipsoids with short dimensions of 7 nm and long dimensions of 11–13 nm, or with a "linear-pearls" model consisting of spherical particles like pearls on a (linear) string [26]. For the linear-pearls model it was assumed that the particles are touching (i.e., no separation) and the diameter was fixed at 7 nm. The best fit was obtained with a combination of short chains of either two (68%) or three pearls (42%). Fit parameters were two-pearl fraction, three-pearl fraction, size polydispersity, background and a scale factor. The polydispersity comes out rather large at 28.3 ± 0.2% probably reflecting that the particles are not accurately described by spheres.

Similarly, the SANS data from the sample with 2.5 mM NaCl (Figure 6b) was modelled well with a cylinder with 7 nm diameter and a length of 74 ± 12 nm or linear pearls model with 9–14 pearls in the chain. The model is not very sensitive to the number of pearls. The best fit was with an 11-pearl model, giving a size-polydispersity of 27.33 ± 0.13%.

The SANS data gives a picture consistent with the TEM and DLS data, with the as-prepared sample consisting of isolated asymmetric particles or short chains and the sample with 2.5 mM NaCl consisting of long chains of ~11 particles on average. The DLS and SANS experiments thus confirm that the linear chains are present in solution and are not merely a consequence of the drying process.

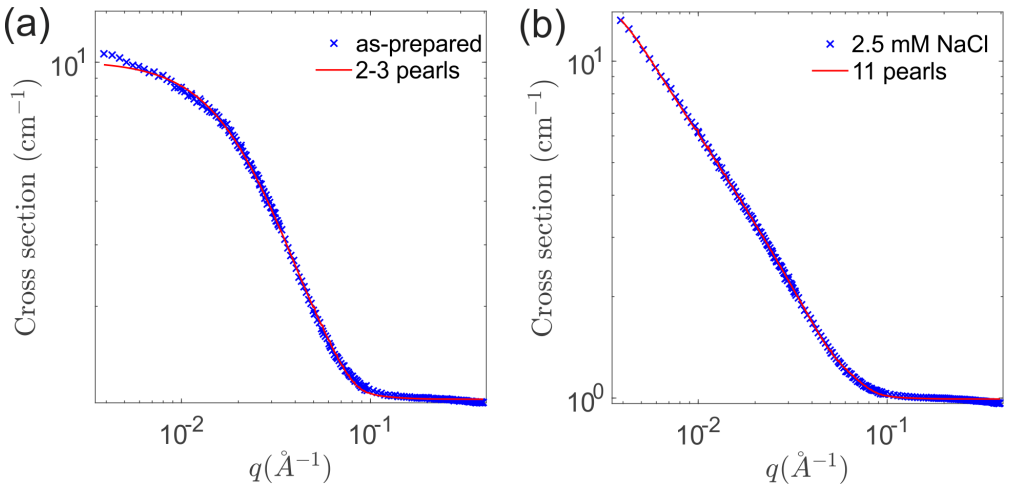

Figure 6. Small angle neutron scattering (SANS) measurements on liquid samples of hematite nanoparticles. (**a**) As-prepared; (**b**) in 2.5 mM NaCl. Blue crosses are data points. Red line is fit to data.

DLS measurements (not shown) of the hematite sample mixed with solutions of NaH_2PO_4 revealed that a concentration of 0.75 mM is needed to initiate aggregation. For concentrations of approximately 2.0 mM and larger, rapid sedimentation occurs. Figure 7 shows TEM images after mixing with 0.75 mM NaH_2PO_4. Although, some chain formation exist, the rather straight, one-particle wide chains of particles, aligned with parallel [001] axes, as seen in case of mixing with NaCl, is not observed. Rather in many cases, we observe the long axis of the particles to be oriented at an angle to the chain when mixed with NaH_2PO_4.

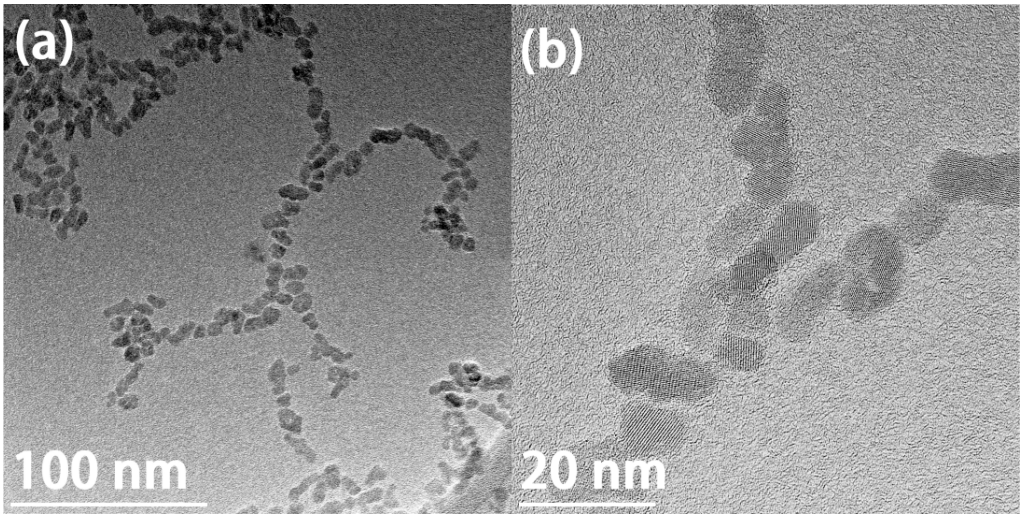

Figure 7. TEM micrographs of hematite nanoparticle sample with 0.75 mM NaH_2PO_4. (**a**) Image of aggregated of hematite particles; (**b**) High-resolution image of aggregated particles.

3.3. Effect or Hydrothermal Treatment: Crystal Growth from Different Aggregation States

Figure 8 shows the change in PSD as function of aging temperature for the samples without NaCl (Figure 8a), with 0.05 mM NaCl (Figure 8b) and 0.5 mM NaCl (Figure 8c).

For the samples without NaCl (Figure 8a) the hydrothermal treatment at 100 °C has the effect of shifting the PSD from d_H = 11.8 ± 5.2 nm to d_H = 12.5 ± 5.2 nm. When the autoclaving temperature

is increased to 120 °C the PSD changes more significantly to d_H = 15.7 ± 6.3 nm. For the sample autoclaved at 140 °C d_H is shifted to even higher sizes and the PSD becomes much broader and the PSD is bimodal with two distributions centered about 18 nm and 73 nm.

From PSDs of the samples with 0.05 mM and 0.5 mM NaCl (Figure 8b,c) it is clear that increasing the concentration of NaCl enhances the effect of the hydrothermal treatment, leading to larger hydrodynamic diameters: With 0.05 mM NaCl the PSDs of the samples heated at 100 °C and 120 °C are shifted towards larger d_H (13.2 ± 5.2 nm and 20.5 ± 7.4 nm) and the PSD of the 140 °C sample is even more polydisperse than the corresponding sample without NaCl and also shifted to higher sizes (d_H = 58 ± 54 nm). For the 0.5 mM NaCl sample the PSDs of the sample heated at 100 °C is further shifted to 19.9 ± 7.5 nm and the PSD of the samples heated at 120 °C and 140 °C are both very broad, ranging over sizes from hundreds to thousands of nanometers.

For the sample with 2.5 mM NaCl the PSD was already very polydisperse before the hydrothermal treatment as shown in Figure 5a and after heating at 140 °C the particles or aggregates were so large that a large fraction of them sedimented during the DLS measurements.

DLS for very polydisperse samples can be problematic and the exact shape of the PSDs should probably not be given too much significance. However, the PSDs can be considered an indication of the ever increasing particle size with salt concentration and autoclaving temperature.

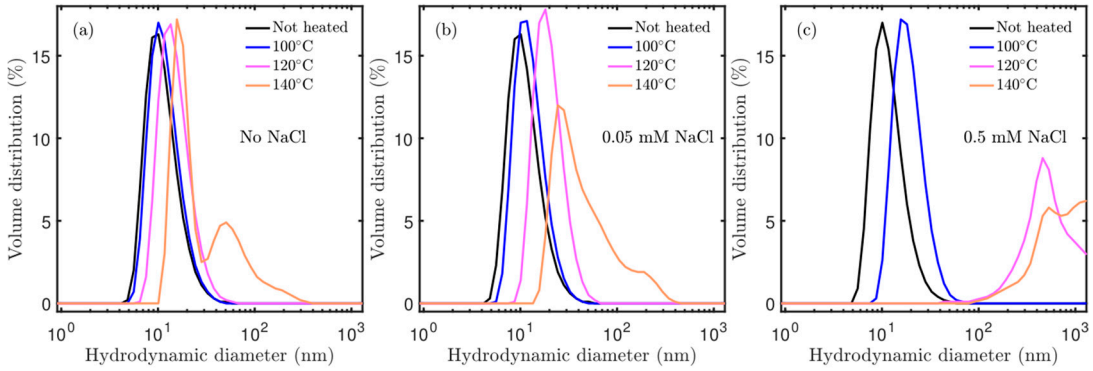

Figure 8. Particle size distributions after autoclaving at the indicated temperatures measured with DLS. (**a**) No NaCl; (**b**) 0.05 mM NaCl; (**c**) 0.5 mM NaCl.

TEM images of the samples heated at 140 °C are shown in Figure 9 for the sample without NaCl (Figure 9a,b) and the sample with 2.5 mM NaCl (Figure 9c,d). From the micrographs it is seen that the shape of individual particles have changed with the heating. Contrary to the particles in Figures 1 and 3, the particles after the hydrothermal treatment often have sharp crystal facets. Particles smaller than 10 nm still exist, but generally the particle size has also increased, especially for the sample aged at 140 °C with 2.5 mM NaCl. For the sample without NaCl heated at 140 °C (Figure 9a,b) the average particle width and length were measured in the same way as for the as-prepared sample in Figure 1 giving particle dimensions of 18 ± 6 nm × 14 ± 4 nm. For the 2.5 mM NaCl sample heated at 140 °C (Figure 9c,d) many particles are larger than 30 nm. After the hydrothermal treatment most particles are collected in aggregates of more than 20 particles while a few particles are still isolated. The particle aggregation could be an effect of the drying, however, DLS shows that there are also large aggregates in the suspension. In the sample heated with 2.5 mM NaCl there are almost no isolated particles and there is no sign of the long linear chains of particles seen in the sample before the hydrothermal treatment.

The sample with 2.5 mM NaCl was, after hydrothermal treatment at 140 °C, characterized by XRD. The diffraction pattern is shown in Figure 10. In comparison with the as-prepared sample, the diffraction peaks have become considerably narrower indicating an increased particle size. An extra phase was included in the refinement to account for the scattering from NaCl in the sample. Again,

data were modeled by a Rietveld refinement. Overall the model represents the data well. There are once again some misfits of the profile shape and there are also two peaks at about 37° and 38° from an unidentified impurity, but no phase conversion of hematite was observed. The refinement results in unit cell parameters of a = 5.0337 ± 0.0006 Å and c = 13.7551 ± 0.0012 Å and a mean particle size of 22.9 ± 0.2 nm. A model with two Lorentzian parameters was also refined to this data giving particles sizes of about 23 nm both parallel and perpendicular to [001].

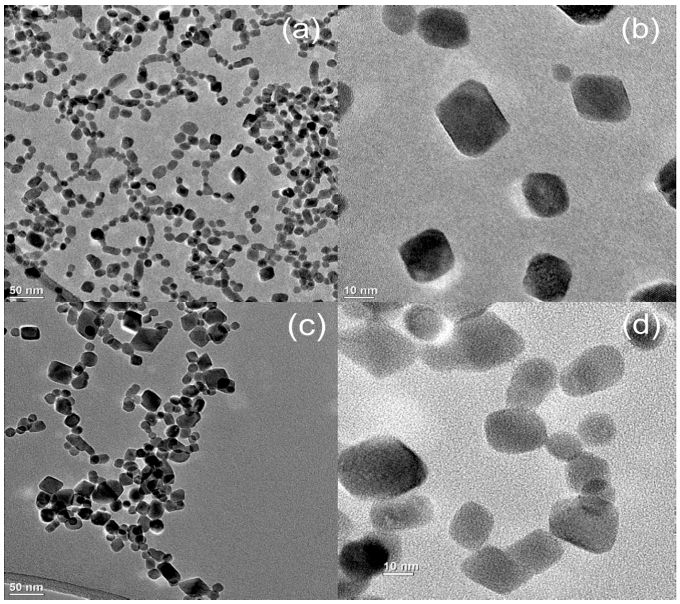

Figure 9. TEM micrographs of samples after hydrothermal treatment at 140 °C. (**a**,**b**) Sample without NaCl; (**c**,**d**) Sample with 2.5 mM NaCl.

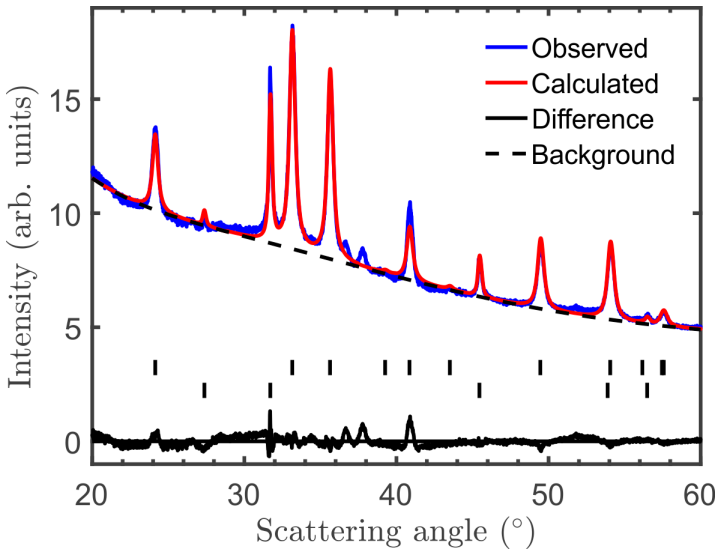

Figure 10. XRD patterns of the 2.5 mM NaCl sample after hydrothermal treatment at 140 °C. The upper tick marks correspond to the hematite structure, the lower to the NaCl structure.

3.4. Magnetic Properties

Mössbauer spectra obtained at 20 K and 80 K of the samples without NaCl added are shown in Figure 11. The 80 K spectrum of the as-prepared sample consists of a broad almost single-line feature which we attribute to hematite nanoparticles being so small that they undergo superparamagnetic

relaxation (this spectral component is a doublet but with two broad lines so closely together that it is effectively a singlet). After hydrothermal treatment at 100 °C, the broad feature still dominates, but a small magnetically split sextet is seen (<20% of the spectrum), most likely due to crystal growth. In the sample heated at 120 °C the sextet component is clearly visible (~50% of the spectrum) and there is an asymmetry between lines 1 and 6, with line 1 being narrower and more intense than line 6. The asymmetry is due to the presence of more than one quadrupole shift, a signature that a Morin transition has occurred in part of the sample, presumably due to crystal growth. For the sample heated at 140 °C, sextet components are dominant, with the superparamagnetic doublet reduced to only ~14% of the spectral area; this spectrum contains two magnetically split components, one with relative spectral area of ~21%, resembling hematite particles with Morin transition, and one sextet (the remaining ~65% of the spectral area) representing magnetically blocked particles without Morin transition.

The spectra of the samples obtained at 20 K are all magnetically split (i.e., the superparamagnetic blocking temperature is above 20 K). The 20 K spectra of the as-prepared sample and the sample heated at 100 °C are fitted with a single sextet with parameters typical of hematite without Morin transition. The 20 K spectra of the samples heated at 120 °C and 140 °C are split into two sextets which indicate, in agreement with the 80 K data, that after the hydrothermal treatment there is a fraction of the particles in the sample that show a Morin transition and further that this fraction increases with heat treatment (~12% in the 120 °C sample, ~30% in the 140 °C sample).

Mössbauer spectra of the samples with 2.5 mM NaCl obtained at 20 K and 80 K are shown in Figure 12. The 80 K spectrum of the sample with 2.5 mM NaCl not subjected to hydrothermal treatment is dominated by a doublet due to superparamagnetic relaxation, but unlike the spectrum of the as-prepared sample there is a clear sextet component in the spectrum, presumably an effect of the aggregation seen by TEM. The 80 K spectrum of the sample with 2.5 mM NaCl heated at 100 °C shows a more distinct sextet component with a relative spectral area of 50%. For the sample with 2.5 mM NaCl heated at 140 °C the 80 K spectrum has no significant doublet component, and the sextet is split into two components with relative spectral areas of ~77% and ~23%, resembling hematite with and without Morin transition, respectively.

The 20 K spectra of the samples with 2.5 mM NaCl are all magnetically split. The spectrum of the 2.5 mM NaCl sample not subjected to hydrothermal treatment consists of a single sextet with hyperfine parameters corresponding to hematite without Morin transition. The spectrum is not much affected by the hydrothermal treatment at 100 °C, but there is a slight increase in the quadruple shift that might indicate that a small proportion of the sample has reached its Morin transition. At 140 °C, the spectrum is clearly split into two sextets with relative spectral areas of ~70% and ~30% in reasonable agreement (within uncertainty) with the result obtained at 80 K (uncertainty is around ±5% on the area determination).

In summary, the Mössbauer data shows a clear connection between aggregation, crystal growth and magnetic properties: Initially, in the case of the as-prepared sample, the particles are superparamagnetic at 80 K, and without Morin transition. These are clear nanoparticle-effects. After aggregation, relaxation is partially suppressed, as seen from the appearance of the sextet component in the 80 K 2.5 mM NaCl spectrum. Similar suppression of superparamagnetic relaxation has been seen before for aggregated antiferromagnetic particles [19–21,27,28], and has been attributed to exchange coupling between surface atoms of neighbouring particles.

The heat treatment of the as-prepared sample and the sample mixed with 2.5 mM NaCl diminishes superparamagnetic relaxation and induces a Morin transition in part of the sample. This is in agreement with growth of the hematite particles beyond 15–20 nm in size as observed by TEM and XRD. Moreover, in agreement with the observations by DLS (Figure 8) and TEM (Figure 9), Mössbauer spectroscopy shows that the addition of NaCl significantly increases the effect of the hydrothermal treatment. After heat treatment in 2.5 mM NaCl at 100 °C, only ~50% of the particles are so small that they are superparamagnetic at 80 K compared to more than 80% for the sample treated without NaCl. Further,

after heat treatment at 140 °C, in 2.5 mM NaCl, ~70% of the hematite has grown to a particle size where it shows a Morin transition, compared to only ~30% when no NaCl was added.

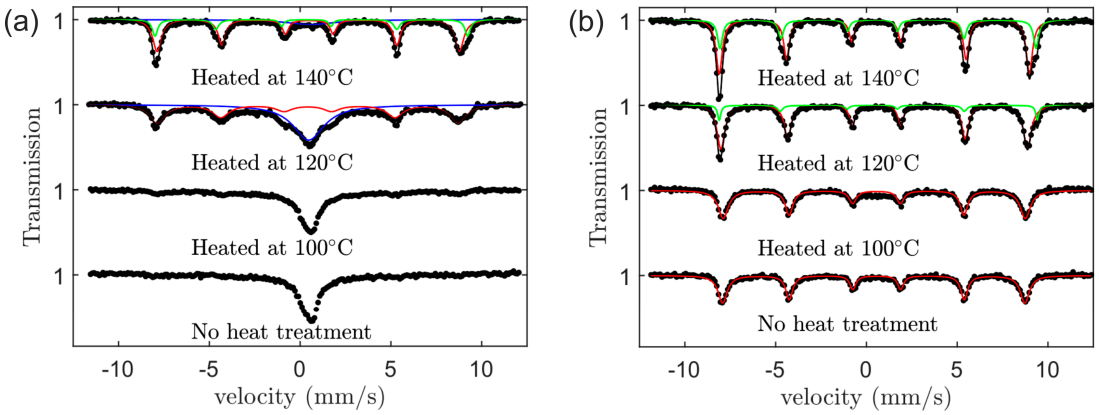

Figure 11. Mössbauer spectra of the as-prepared sample (without NaCl) heated at the indicated temperatures. (**a**) Measurement at 80 K; (**b**) Measurement at 20 K. Fit to the superparamagnetic doublet is plotted in blue, and sextets for hematite with and without Morin transition are plotted in green and red, respectively.

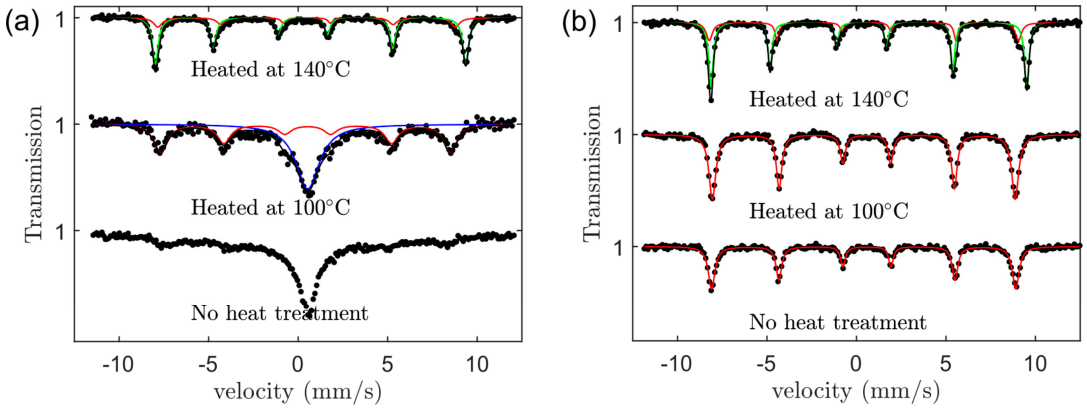

Figure 12. Mössbauer spectra of the hematite sample with 2.5 mM NaCl heated at the indicated temperatures. (**a**) Measurement at 80 K; (**b**) Measurement at 20 K. Fit to the superparamagnetic doublet is plotted in blue, and sextets for hematite with and without Morin transition are plotted in green and red, respectively.

4. Discussion

From TEM, DLS, SANS and Mössbauer spectroscopy measurements we have observed that adding NaCl in concentration of 2.5 mM to the acidic suspensions of hematite nanoparticles leads to aggregation of the particles. The effect of adding NaCl is a neutralization of the charge on the hematite particles by the salt ions [14]. With TEM we have seen that the addition of NaCl solution to the suspension of hematite nanoparticles may lead to the formation of straight chains of these particles. The resulting structures represent a kind of one-dimensional mesocrystals [4,5]. TEM further provides clear evidence that the particles in the chains often are crystallographically aligned with parallel [001] axes, even though they are not fused together. The chains of crystallographically aligned particles seem to be very stable (for months) in solution once formed (possibly over days to weeks). Previous work has shown that it is possible to separate hematite nanoparticles, which have aggregated (not coalesced) due to drying, by use of grinding or ultrasonic treatment [29], but in the present study no mechanical (or chemical) tests were made on the stability of the suspended chains.

One could speculate that for instance Cl^- ions attach to the particles preferentially on certain crystallographic surfaces, e.g., specifically (001), and facilitate the preferred arrangement of the particles, as sketched in Figure 13a. Adsorption of Cl^- to specific faces of hematite has previously been proposed by e.g., Sugimoto et al. [9]. In contrast the addition of NaH_2PO_4 solution, which also drives aggregation, do not lead to particles preferentially aligned along their [001] axes. Addition of NaH_2PO_4 has previously been shown to lead to different crystal morphologies than e.g., chloride ions during crystal growth [9] possibly because the ions adsorb to different surfaces.

Data further shows that the induced aggregation enhances the effect of the hydrothermal treatment, presumably because the change in ionic strength brings the particles closer together, facilitating sintering of the particles (as compared to samples without salt added, cf. Figure 13b). The particle growth may be ascribed to both particle migration and coalescence and atomic migration between particles (Ostwald ripening). TEM images show that the effect of the hydrothermal treatment is growth of the individual particles and a change of shape from pseudo-spherical to faceted. The faceting is presumably because the thermal energy makes the atoms more mobile and their random motion leads to the shape of the nanocrystals converging towards their equilibrium shape, with the faces with highest surface energies least exposed.

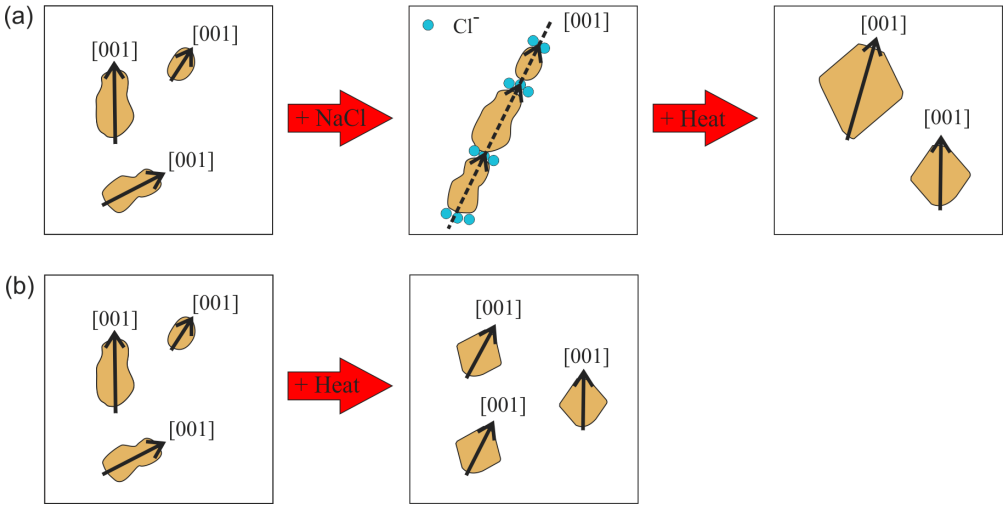

Figure 13. Model of aggregation and crystal growth. (**a**) Oriented alignment assisted by Cl^- ions attached to (001) surfaces of the particles which lead to linear chains, like observed in the TEM images of the sample with 2.5 mM NaCl, followed by enhanced crystal growth during heat treatment. We have not observed if any ions are sitting on the (001) particles surfaces so the model is speculative; (**b**) Crystal growth of the heated samples without salt.

5. Conclusions

In the present study we have found that addition of NaCl to a suspension of well dispersed ~8 nm hematite particles can lead to mesocrystal arrangement of the particles into long linear chains with parallel [001] axes. Neighbouring particles are crystallographically aligned but not directly connected. We speculate that the aggregation of particles into these one-dimensional mesocrystals could be associated with preferential attachment of Cl^- ions on the (001) surfaces of the hematite particles. We find that this mesocrystal structure leads to a partial suppression of the superparamagnetic relaxation of the hematite nanoparticles. As the particles are antiferromagnetic with negligible dipolar interactions, the suppression is possibly due to exchange coupling between the particles. Conceivably, the Cl^- ions on the surface of particles could mediate the coupling. Hydrothermal treatment at 100–140 °C leads to growth of the individual particles beyond 15–20 nm. The growth induces a Morin transition in a fraction of the particles and this effect increases with autoclaving temperature. Since

the Morin transition is only induced in samples subjected to hydrothermal treatment it is probably an effect of the growth of single particles and not of magnetic order extended over several particles in the mesocrystal-like aggregates. TEM measurements confirm that samples with Morin transition have a significant fraction of particles with sizes larger than 20 nm. Although addition of NaCl to the particle suspension does not itself induce a Morin transition it does increase the effect of the hydrothermal treatment, leading to a higher fraction of the sample undergoing Morin transition. This can be understood by a reduction of the ionic strength allowing the particles to come closer together and form mesocrystals which more readily fuse together to form larger single crystals upon heating.

Acknowledgments: We acknowledge funding from the Danish Council for Independent Research. Our work benefitted from the SasView software, originally developed by the DANSE project under NSF award DMR-0520547.

Author Contributions: E.B. and C.F. designed the experiments and wrote most of the paper. E.B. lead the samples preparation, experimental studies (TEM, XRD, DLS, SANS, Mössbauer spectroscopy) and data analysis, and worked together with M.V. (sample preparation, DLS), J.L. (Mössbauer spectroscopy, TEM), and T.W.H. (TEM). All authors contributed to discussion of the results and the writing of the paper.

Conflicts of Interest: The authors declare no conflict of interest. The identification of any commercial product or trade name does not imply endorsement or recommendation by the National Institute of Standards and Technology. The founding sponsors had no role in the design of the study; in the collection, analyses, or interpretation of data; in the writing of the manuscript, and in the decision to publish the results.

References

1. Penn, R.L.; Banfield, J.F. Morphology development and crystal growth in nanocrystalline aggregates under hydrothermal conditions: Insights from titania. *Geochim. Cosmochim. Acta* **1999**, *63*, 1549–1557. [CrossRef]
2. Penn, R.L.; Banfield, J.F. Imperfect oriented attachment: Dislocation generation in defect-free nanocrystals. *Science* **1998**, *281*, 969–971. [CrossRef] [PubMed]
3. Zhang, H.; De Yoreo, J.J.; Banfield, J.F. A Unified description of attachment-based crystal growth. *ACS Nano* **2014**, *8*, 6526–6530. [CrossRef] [PubMed]
4. Niederberger, M.; Cölfen, H. Oriented attachment and mesocrystals: Non-classical crystallization mechanisms based on nanoparticle assembly. *Phys. Chem. Chem. Phys.* **2006**, *8*, 3271–3287. [CrossRef] [PubMed]
5. Zhang, J.; Huang, F.; Lin, Z. Progress of nanocrystalline growth kinetics based on oriented attachment. *Nanoscale* **2010**, *2*, 18–34. [CrossRef] [PubMed]
6. Li, D.; Nielsen, M.H.; Lee, J.R.I.; Frandsen, C.; Banfield, J.F.; De Yoreo, J.J. Direction-specific interactions control crystal growth by oriented attachment. *Science* **2012**, *336*, 1014–1018. [CrossRef] [PubMed]
7. Pfeiffer, C.; Rehbock, C.; Hühn, D.; Carrillo-Carrion, C.; de Aberasturi, D.J.; Merk, V.; Barcikowski, S.; Parak, W.J. Interaction of colloidal nanoparticles with their local environment: The (ionic) nanoenvironment around nanoparticles is different from bulk and determines the physico-chemical properties of the nanoparticles. *J. R. Soc. Interface* **2014**, *11*, 20130931. [CrossRef] [PubMed]
8. Oncsik, T.; Trefalt, G.; Borkovec, M.; Szilagyi, I. Specific ion effects on particle aggregation induced by monovalent salts within the Hofmeister series. *Langmuir* **2015**, *31*, 3799–3807. [CrossRef] [PubMed]
9. Sugimoto, T.; Wang, Y.; Itoh, H.; Muramatsu, A. Systematic control of size, shape and internal structure of monodisperse α-Fe_2O_3 particles. *Colloids Surf. A Physicochem. Eng. Asp.* **1998**, *134*, 265–279. [CrossRef]
10. Sugimoto, T.; Wang, Y. Mechanism of the Shape and Structure Control of Monodispersed α-Fe_2O_3 Particles by Sulfate Ions. *J. Colloid Interface Sci.* **1998**, *207*, 137–149. [CrossRef] [PubMed]
11. Sugimoto, T.; Muramatsu, A. Formation Mechanism of monodispersed α-Fe_2O_3 particles in dilute $FeCl_3$ solutions. *J. Colloid Interface Sci.* **1996**, *184*, 626–638. [CrossRef] [PubMed]
12. Reeves, N.J.; Mann, S.; Heller, W.; Docherty, R.; Bils, R.; Saltman, P. Influence of inorganic and organic additives on the tailored synthesis of iron oxides. *J. Chem. Soc. Faraday Trans.* **1991**, *87*, 3875. [CrossRef]
13. Livage, J.; Henry, M.; Sanchez, C. Sol-gel chemistry of transition metal oxides. *Prog. Solid State Chem.* **1988**, *18*, 259–341. [CrossRef]
14. He, Y.T.; Wan, J.; Tokunaga, T. Kinetic stability of hematite nanoparticles: The effect of particle sizes. *J. Nanopart. Res.* **2008**, *10*, 321–332. [CrossRef]

15. Morrish, A.H. *Canted Antiferromagnetism: Hematite*; World Scientific: Singapore, 1994; ISBN 9810220073.
16. Besser, P.J.; Morrish, A.H.; Searle, C.W. Magnetocrystalline anisotropy of pure and doped hematite. *Phys. Rev.* **1967**, *153*, 632–640. [CrossRef]
17. Yamamoto, N. The Shift of the spin flip temperature of α-Fe_2O_3 fine particles. *J. Phys. Soc. Jpn.* **1968**, *24*, 23–28. [CrossRef]
18. Varón, M.; Beleggia, M.; Kasama, T.; Harrison, R.J.; Dunin-Borkowski, R.E.; Puntes, V.F.; Frandsen, C. Dipolar magnetism in ordered and disordered low-dimensional nanoparticle assemblies. *Sci. Rep.* **2013**, *3*, 1234. [CrossRef] [PubMed]
19. Hansen, M.F.; Koch, C.B.; Mørup, S. Magnetic dynamics of weakly and strongly interacting hematite nanoparticles. *Phys. Rev. B* **2000**, *62*, 1124–1135. [CrossRef]
20. Frandsen, C.; Mørup, S. Inter-particle interactions in composites of antiferromagnetic nanoparticles. *J. Magn. Magn. Mater.* **2003**, *266*, 36–48. [CrossRef]
21. Frandsen, C.; Bahl, C.R.H.; Lebech, B.; Lefmann, K.; Kuhn, L.T.; Keller, L.; Andersen, N.H.; Zimmermann, M.V.; Johnson, E.; Klausen, S.N.; et al. Oriented attachment and exchange coupling of α-Fe_2O_3 nanoparticles. *Phys. Rev. B* **2005**, *72*, 214406. [CrossRef]
22. Gilbert, B.; Frandsen, C.; Maxey, E.R.; Sherman, D.M. Band-gap measurements of bulk and nanoscale hematite by soft X-ray spectroscopy. *Phys. Rev. B* **2009**, *79*, 35108. [CrossRef]
23. Kline, S.R. Reduction and analysis of SANS and USANS data using IGOR Pro. *J. Appl. Crystallogr.* **2006**, *39*, 895–900. [CrossRef]
24. SasView for Small Angle Scattering Analysis. Available online: http://www.sasview.org (accessed on 15 June 2017).
25. Howard, C.J.; Hill, R.J. *AAEC (now ANSTO) Report M112*; Lucas Heights Research Laboratory: Lucas Heights, Australia, 1986.
26. Dobrynin, A.V.; Rubinstein, M.; Obukhov, S.P. Cascade of transitions of polyelectrolytes in poor solvents. *Macromolecules* **1996**, *29*, 2974–2979. [CrossRef]
27. Frandsen, C.; Lefmann, K.; Lebech, B.; Bahl, C.R.H.; Brok, E.; Ancoña, S.N.; Theil Kuhn, L.; Keller, L.; Kasama, T.; Gontard, L.C.; et al. Spin reorientation in α-Fe_2O_3 nanoparticles induced by interparticle exchange interactions in α-Fe_2O_3/NiO nanocomposites. *Phys. Rev. B* **2011**, *84*, 214435. [CrossRef]
28. Brok, E.; Frandsen, C.; Madsen, D.E.; Jacobsen, H.; Birk, J.O.; Lefmann, K.; Bendix, J.; Pedersen, K.S.; Boothroyd, C.B.; Berhe, A.A.; et al. Magnetic properties of ultra-small goethite nanoparticles. *J. Phys. D Appl. Phys.* **2014**, *47*, 365003. [CrossRef]
29. Frandsen, C.; Mørup, S. Reversible aggregation and magnetic coupling of α-Fe_2O_3 nanoparticles. *J. Phys. C Condens. Matter* **2006**, *18*, 7079. [CrossRef]